

1 NATURAL VARIATION IN ENSO FLAVORS

2 Matthew Newman^{1,3}, Sang-Ik Shin², and Michael A. Alexander³

3 ¹CIRES Climate Diagnostics Center, University of Colorado, Boulder, Colorado

4 ²College of Marine Science, University of South Florida

5 ³Physical Sciences Division/NOAA Earth System Research Laboratory, Boulder, Colorado

6

7 Email: matt.newman@noaa.gov

8 Revision submitted to *Geophysical Research Letters* Monday, May 16, 2011

9

10 ABSTRACT

11 Using a multivariate, “patterns-based”, red noise approach to 42 years of observed tropical SST,
12 thermocline depth, and zonal wind stress seasonal anomalies, it is shown that natural random
13 variations can account for the observed variability of Central Pacific (CP) and Eastern Pacific
14 (EP) ENSO events. The recent multidecadal increase in the number of CP events relative to EP
15 events, which has been hypothesized to be connected to anthropogenic change in the state of the
16 ocean, is also found to be consistent with multivariate red noise and hence with stationary
17 statistics. ENSO “flavors” are the consequence of differing combinations of two initially
18 orthogonal spatial patterns that are precursors to CP or EP events of both signs. These precursors
19 can be excited by random weather forcing and subsequently result in SST anomaly amplification
20 primarily through surface or thermocline feedbacks, respectively.

21

22 **1) Introduction**

23 El Niño-Southern oscillation (ENSO), the dominant tropical coupled atmosphere-ocean
24 phenomenon on interannual time scales, impacts the climate not only over the tropics but also
25 over the globe [e.g. *Alexander et al.*, 2002]. Historically, El Niño has been defined as the
26 appearance of warm sea surface temperature (SST) anomalies in the eastern tropical Pacific
27 including the “Niño3” region (5°S-5°N and 150°W-90°W). However, some El Niño events,
28 particularly recently, have maximum SST anomalies located primarily in the central tropical
29 Pacific “Niño4” region (5°S-5°N and 160°E-150°W), with attendant shifts in both atmospheric
30 teleconnections and their worldwide impacts compared to the canonical ENSO [e.g. *Ashok et al.*,
31 2007; *Kim et al.*, 2009; *Yeh et al.*, 2009; *Di Lorenzo et al.*, 2010; *Mo*, 2010; *Yu and Kim*, 2011].

32 It has long been recognized that each El Niño event may have differences in detail from
33 the standard composite during the course of its evolution; this has sometimes been referred to as
34 different ENSO “flavors” and can be represented, for example, by secondary ENSO indices
35 representing east-west SST differences [e.g. *Trenberth and Stepaniak*, 2001]. This diverse El
36 Niño evolution received much attention recently after *Yeh et al.*'s [2009] analysis of El Niño in
37 the IPCC AR4 future climate projections suggested that increasing “CP-El Niño” occurrence
38 could be a response to ongoing greenhouse warming. In their nomenclature, an EP-El Niño (CP-
39 El Niño) event occurs when the Niño3 (Niño4) SST anomaly is greater than 0.5°C and greater
40 than the Niño4 (Niño3) anomaly. Observational studies suggesting that CP-El Niño has
41 increasingly become the dominant form of El Niño since the late 1960s have also raised the
42 possibility that some natural and/or anthropogenic “base state” change (that is, a substantial
43 difference in the ocean mean state that alters stability properties) has changed characteristic El
44 Niño evolution [*Yeh et al.*, 2009; *Lee and McPhaden*, 2010]. On the other hand, using the 4200

45 year long Kiel Climate Model simulations, *Yeh et al.* [2011] showed that the frequency of CP-El
46 Niño occurrence can increase without any changes in radiative forcings, and acknowledged that
47 an increasing frequency of CP-El Niño occurrence may also be consistent with natural climate
48 variability. However, considering the deficient simulations of El Niño in coupled climate models
49 [*Guilyardi et al.*, 2009; *Newman et al.*, 2009; *Yu and Kim*, 2010], the latter conclusion may also
50 be highly model dependent (see Fig. 3 of *Yeh et al.* [2009]).

51 The questions raised by these studies can be summarized as: 1) does the recent increase
52 in CP ENSOs reflect decadal base state change? and 2) does the recent increase in CP ENSOs
53 reflect anthropogenic change? To answer these questions, it is important to first construct a
54 suitable null hypothesis against which both observational and modeling studies may be tested:
55 *observed changes in ENSO characteristics are consistent with natural seasonal variability with*
56 *stationary statistics.* A standard null hypothesis in climate studies is to compare the variability of
57 a time series, either of an index or of a value at a fixed location, to scalar “red noise”. We
58 suggest that when testing changing relationships between multiple indices, or more generally the
59 variability of a series of evolving maps, the appropriate comparison is to multivariate red noise.
60 In this paper, using statistically stationary multivariate red noise determined from observed
61 tropical SST, thermocline depth, and zonal wind stress seasonal anomalies, we find the expected
62 multidecadal range in the relative frequency and amplitude of CP and EP ENSO events and
63 compare this range to what has so far been either observed or projected to occur.

64 **2) “Patterns-based” multivariate red noise**

65 Climate variability is often characterized by a notable separation between the dominant
66 time scales of interacting processes. For example, compared to the much longer timescales of the
67 ocean, weather varies so rapidly that it can be considered to have almost no memory. Weather

68 forcing of the oceanic mixed layer can then be approximated as white noise forcing of a damped
69 integrator [e.g., *Hasselmann*, 1976]. This is an example of *univariate red noise* (also called an
70 AR1 process) for an anomaly scalar time series $x(t)$, the simplest null hypothesis for both
71 atmospheric and oceanic climate variability [e.g., *Wunsch*, 1999; *Rudnick and Davis*, 2003].

72 When extended to the more general case of an anomaly state vector $\mathbf{x}(t)$ representing
73 many evolving regional patterns of climate variables, this approximation based on time scale
74 separation becomes *multivariate red noise*,

$$75 \quad 1) \quad \frac{d\mathbf{x}}{dt} = \mathbf{L}\mathbf{x} + \boldsymbol{\xi}$$

76 [e.g., *Penland and Sardeshmukh*, 1995], with two notable differences from univariate red noise.
77 First, \mathbf{L} is a two-dimensional damped linear operator representing both local and non-local
78 dynamics, including interactions between variables, so multivariate red noise represents the
79 evolution of both stationary and propagating anomaly patterns (i.e., eigenmodes of \mathbf{L}); scalar
80 indices derived from \mathbf{x} can then have spectral peaks [e.g., *Newman*, 2007]. Second, some
81 characteristic physical processes operate mostly in one direction – for example, atmospheric
82 wind stress directly drives ocean circulation and thermocline changes but not vice versa [e.g.,
83 *Moore and Kleeman*, 1999] – so \mathbf{L} does not have symmetric dynamical relationships between all
84 elements of \mathbf{x} . Consequently, despite the lack of exponential modal instability, some anomalies
85 experience significant but transient growth over finite time intervals (i.e., \mathbf{L} is stable but non-self
86 adjoint; e.g., *Farrell* [1988]), since anomalies that are initially best configured to grow also
87 evolve into new patterns and/or move into new regions that lead to decay. These “optimal
88 structures” [e.g., *Penland and Sardeshmukh*, 1995] are initiated by some realizations of the
89 unpredictable white noise $\boldsymbol{\xi}$, which has spatial but no temporal coherence.

90 The empirical method that determines multivariate red noise from observations is Linear
91 Inverse Modeling [LIM; *Penland and Sardeshmukh*, 1995]. In this paper, we use the LIM
92 developed by *Newman et al.* [2011; hereafter NAS], in which \mathbf{x} consists of 3-month running
93 mean anomalies of observed SST [*Rayner et al.*, 2003], thermocline depth (depth of 20°C
94 isotherm) [*Carton and Giese*, 2008], and surface zonal wind stress [*Kalnay et al.*, 1996] in the
95 Tropics (30°S-30°N) during 1959-2000. We integrated (1) forwards for 24000 yrs, treating it as a
96 stochastically-forced dynamical model following NAS. Repeating our study using detrended data
97 yielded negligible differences in all results reported below.

98 **3) Distinguishing CP and EP events within multivariate red noise**

99 NAS verified multivariate red noise with tests ensuring that when (1) is determined from
100 a specified lag (here, 3 months) it accurately reproduces observed evolution statistics at much
101 longer time scales. Here we verify that CP and EP ENSO variations are reproduced by
102 multivariate red noise. First, Niño3 and Niño4 power spectra determined by (1) are compared to
103 the observed spectra in **Figure 1**. The multivariate red noise and observed spectra closely match,
104 with a strongly significant peak in the 2-7 year band and small deviations that are not statistically
105 significant. In contrast, the spectra of virtually all ensemble members of the “20th-century”
106 (20c3m) IPCC AR4 coupled GCMs lie substantially outside the 95% confidence interval [see
107 *Newman et al.*, 2009]. Additionally, Fig. 1c shows that the simultaneous and lagged correlation
108 between Niño3 and Niño4, $r(\text{Niño3}, \text{Niño4})$, determined from (1) compares quite well with the
109 observed $r(\text{Niño3}, \text{Niño4})$. Note that if Niño3 and Niño4 were instead each independently fitted
110 with univariate red noises, their expected correlation would be zero.

111 Second, in **Figure 2** we show the two optimal structures leading to SST amplification
112 over an interval of six months. (This interval is chosen as a compromise between 9 months, the

113 time of peak growth for the leading optimal, and 4 months, the peak for the second optimal.) The
114 leading optimal structure (Fig. 2a) leads to the maximum possible amplification of rms SST
115 anomaly within the entire tropical domain, and the second optimal structure (Fig. 2b) is
116 orthogonal to the leading one at both $t = 0$ and $t = 6$ months. The evolution of both is shown in
117 the Hovmollers at the bottom of each column. The leading optimal structure evolves into an “EP-
118 ENSO” event. It is quite similar to the optimal structure for growth over nine months discussed
119 by NAS, who also used a diagnosis of the feedbacks within \mathbf{L} to show how this structure’s
120 observed evolution is driven by both surface and thermocline interactions [see also *Neelin et al.*,
121 1998], with the zonally averaged thermocline anomaly decreasing to zero as the amplitude of the
122 SST anomaly maximizes, and subsequent decay and sign change as in the classic “recharge-
123 discharge” mechanism [*Jin*, 1997]. In contrast, the second optimal structure (which has not been
124 studied before) evolves into a “CP-ENSO” event with \mathbf{L} initially driving growth through “non-
125 local” interactions within SST (e.g., advection of SST anomalies; see Fig. 4b of NAS). In
126 particular, the initial equatorial heat content anomaly is near zero and there is no recharge-
127 discharge mechanism, also suggested by some other studies of warm CP events [*Kao and Yu*,
128 2009; *Kug et al.*, 2009]. Thus, although the SST anomaly grows fairly weakly, the lack of the
129 discharge mechanism also slows its decay, allowing the anomaly to persist relatively longer than
130 does the EP ENSO. This evolution of the CP optimal is consistent with NAS who suggested that
131 without thermocline-surface interactions, overall SST variability would be weaker but also more
132 persistent, and shifted west towards the central Pacific. In its second year the CP optimal
133 evolution weakens slightly but then strengthens to the east, behavior characteristic of the multi-
134 year CP events, as the thermocline anomaly evolves so that its feedback on SSTs becomes more
135 important, especially further east.

136 The projection of observed anomalies on the initial optimal structures is compared to the
137 projection of observed SST anomalies upon the corresponding predicted evolved structures 6
138 months later in **Figure 3**. The high linear correlation of these projections for each initial/evolved
139 pair indicates that this *potential* optimal SST growth *does occur* as expected from multivariate
140 red noise; that is, the case-to-case evolution of anomalies is well captured by (1), with the slopes
141 of the least square lines matching the expected amplification factors, plus some remaining scatter
142 due to noise. In contrast to earlier studies suggesting that CP events are warm phase only [e.g.
143 *Kug et al.*, 2009], Fig. 3b shows that CP-ENSO events of both signs occur [as in *Yu and Kim*,
144 2011], which is also seen in separate positive and negative composites constructed from SST
145 anomalies six months following all dates on which either the EP-ENSO or CP-ENSO optimal
146 structure amplitudes exceeded 1 standard deviation (blue dots in Figs. 3a and b). The EP [CP]
147 composite in Figs. 3c and e [Figs. 3d and f] is consistent with the expected six-month evolution
148 of the leading [second] optimal pattern. Anomalies with initially high projection on both optimal
149 patterns (indicated by green dots) evolve in a correspondingly mixed manner (not shown).
150 Moreover, no trend exists in the time series of either the CP optimal or evolved pattern; the EP
151 optimal and evolved pattern time series have weak trends that are not significant.

152 **4) Variations of EP and CP events driven by noise**

153 Given that multivariate red noise matches the observed interannual variability of both EP
154 and CP events in the Tropics, we can now assess the potential range of EP and CP variability
155 over multidecadal epochs, assuming no underlying change in either the dynamics or the overall
156 statistics of noise. Using the DJF mean each year of the 24000-year integration we computed the
157 same statistical measures as *Yeh et al.* [2009]: the simultaneous value of $r(\text{Niño}3, \text{Niño}4)$, and
158 the occurrence ratio of CP/EP El Niño (i.e., warm event only) defined as the ratio of CP-El Niño

159 to EP-El Niño events, using Yeh et al's classifications noted in section 1. Results for the full
160 integration are shown in **Figure 4a**, where both measures are determined from 30-yr long
161 intervals centered 10 years apart. Ranges of values for the integration are summarized in **Table 1**
162 by determining 95% confidence bounds from the large number of samples, with sensitivity to the
163 interval size determined by recomputing both measures using non-overlapping (i.e., adjacent) 10,
164 30, 50, or 100-yr intervals. As expected, shorter intervals show much greater variations in EP
165 and CP events. In fact, it is possible to go up to 28 years between EP-El Niño events, and about
166 one in seven 30-yr intervals have no CP-El Niño events. But even over centennial time scales
167 long-term trends in ENSO characteristics are possible simply due to variations in noise.
168 Moreover, any change in long-term mean now is a *residual* of the variability, not a driver of it;
169 for example, for 30-yr means a two standard deviation decrease of EP events results in a
170 deepening of the equatorial thermocline of ~6 m in the central Pacific. These results suggest that
171 even several decades of data may be insufficient to gain an adequate picture of potential
172 externally forced trends in CP/EP variability.

173 For comparison, the same measures determined from three different SST datasets for the
174 years 1891-2010 are shown in Fig. 4c, where again (now due to limited data) the 30-yr intervals
175 have 10-yr overlaps. [Note that for both NOAA datasets, there are no CP events prior to the
176 1941-1970 interval.] Clearly, the potential range in both measures is larger than appears in the
177 SST datasets, even when we repeat these calculations using nonoverlapping 10-yr time intervals
178 (not shown). Of course, the frequency of CP-El Niño occurrence before 1960 is more uncertain
179 due to the lack of long-term SST observations, especially over the central and eastern tropical
180 Pacific Ocean [*Deser et al.*, 2010; *Giese et al.*, 2010], but additional earlier CP events would
181 only decrease the displayed 20th century range. Moreover, a number of 120-yr long periods in the

182 integration mimic the observational record. For example, we define “increasing CP/EP cases” in
183 the integration as two adjacent 60-year segments for which the CP/EP ratio rises from below
184 normal to above normal, and simultaneously $r(\text{Niño3}, \text{Niño4})$ decreases, from the first 60-yr
185 segment to the second. Figure 4b shows that both measures averaged over only these 120-yr
186 periods correspond quite well to Fig. 4c.

187 **5) Concluding remarks**

188 Since multivariate red noise determined from observations provides an excellent baseline
189 for the statistics of observed tropical seasonal anomaly evolution, and particularly differentiates
190 between CP and EP ENSO events, it serves as a useful null hypothesis against which possible
191 changes in the nature of ENSO can be tested. In this case, all past variations in CP and EP ENSO
192 events, at least as determined from current SST gridded datasets, as well as projected changes
193 based on the SRES A1B scenario in the IPCC AR4 models [Yeh *et al.*, 2009; cf. their Fig. 3 to
194 our Fig. 4], appear to be less than may be expected from natural random variability. Note that
195 these results assume statistical stationarity; that is, large multidecadal changes in relative CP and
196 EP ENSO occurrence are consistent with fixed statistics of the 1959-2000 period, with no “base
197 state” change. Also, there was no trend mode (either temporal or spatial) within the CP optimal
198 pattern. Obviously, some variation in these results is likely since \mathbf{L} is only an approximation of
199 the underlying \mathbf{L} that would be determined from a longer period of data. The key point is that we
200 are restricted not by an accounting of CP and EP events that have occurred in the past forty years
201 but rather by the *average simultaneous and 3-month lagged relationships* between the variables
202 and locations represented in our chosen state vector, which allow for the possibility of EP and
203 CP events that are initiated and evolve in a manner consistent with these statistics but have not
204 (yet) occurred.

205 While CP and EP ENSOs may be randomly initiated, this study does suggest that their
206 observed differences represent real dynamical differences in which the dominant physical
207 processes depend on initial conditions, leading to CP ENSOs that may amplify less but also
208 persist more than EP ENSOs. Of course, generally climate anomalies will not exactly project on
209 either of the two optimal structures shown in Fig. 2. Rather, since these structures are orthogonal,
210 an anomaly that is some combination of these two would evolve as a linear combination (plus
211 additional noise subsequent to the initial time). Consequently, many additional “flavors” of
212 ENSO are possible; for example, adding equal amounts of the two initial patterns would lead to a
213 sub-optimal but more persistent ENSO. Given the strong relationships between initial and
214 evolved patterns in Fig. 3, these ENSO flavors and their global impacts should be predictable.

215 It remains possible that anthropogenic forcing might drive a change in the dynamics and
216 hence a change in ENSO as suggested by *Yeh et al.* (2009), but that this change is too small to be
217 significant in the face of short data sets and far smaller model ensembles than are needed to
218 discern it from natural variability [e.g., *Coelho and Goddard*, 2009; *Solomon and Newman*,
219 2011; *Deser et al.*, 2011]. Or anthropogenic effects might drive changes in dominant noise
220 spatial structures rather than in the base state dynamics, which could still change ENSO
221 characteristics. It may be some years, however, before we can determine from data if this is
222 likely.

223

224 **Acknowledgements.** The authors thank an anonymous reviewer and N Schneider for helpful
225 comments. This work was partially supported by the NOAA OAR CVP Program.

226

227 REFERENCES

- 228 Alexander, M. A. et al., (2002), The atmospheric bridge: the influence of ENSO teleconnections
229 on air-sea interaction over the global oceans, *J. Climate*, *15*, 2205-2231.
- 230 Ashok, K., S. K. Behera, S. A. Rao, H. Weng, and T. Yamagata (2007), El Niño Modoki and its
231 possible teleconnection, *J. Geophys. Res.*, *112*, C11007, doi:10.1029/2006JC003798.
- 232 Carton JA, Giese BS (2008) A reanalysis of ocean climate using Simple Ocean Data
233 Assimilation (SODA), *Mon. Wea. Rev.* *136*, 2999-3017.
- 234 Coelho, C.A.S., and L. Goddard (2009): El Nino-induced tropical droughts in climate change
235 projections, *J. Climate*, *22*, 6456-6476.
- 236 Deser, C., A. S. Phillips, and M. A. Alexander (2010), Twentieth century tropical sea surface
237 temperature trends revisited, *Geophys. Res. Lett.*, *37*, L10701, doi:10.1029/2010GL043321.
- 238 Deser, C., A. S. Phillips, V. Bourdette, and H. Teng (2011), Uncertainty in climate change
239 projections: The role of internal variability, *Climate Dyn.*, DOI 10.1007/s00382-010-0977-x.
- 240 Di Lorenzo et al. (2010), Central Pacific El Niño and decadal climate change in the North
241 Pacific, *Nature Geosciences*, *3*, 762-765.
- 242 Farrell B. (1988), Optimal excitation of neutral Rossby waves, *J. Atmos Sci*, *45*, 163-172.
- 243 Giese, B. S et al. (2010), The 1918/1919 El Niño, *Bull Amer. Meteor. Soc.*, *91*, 177-183, DOI:
244 10.1175/2009BAMS2903.1.
- 245 Guilyardi E. et al. (2009), Understanding El Niño in ocean-atmosphere general circulation
246 models: progress and challenges, *Bull Amer. Meteor. Soc.*, *90*, 325-340.
- 247 Hasselmann K. (1976), Stochastic climate models. Part I. Theory, *Tellus*, *28*, 474-485.
- 248 Jin, F-F. (1997), An equatorial ocean recharge paradigm for ENSO. Part I: Conceptual model, *J.*
249 *Atmos. Sci.*, *54*, 811-829.

250 Kalnay E, et al (1996), The NCEP/NCAR 40-Year Reanalysis Project, *Bull. Amer. Meteor. Soc.*,
251 77, 437–471.

252 Kao, H.-Y., and J.-Y. Yu (2009), Contrasting eastern-Pacific and central-Pacific types of ENSO,
253 *J. Climate*, 22, 615–632.

254 Kim, H. M., P. J. Webster, and J. A. Curry (2009), Impact of shifting patterns of Pacific Ocean
255 warming events on North Atlantic Tropical Cyclones, *Science*, 325, 77-80.

256 Kug, J.-S., F.-F. Jin, and S.-I. An (2009), Two types of El Niño events: cold tongue El Niño and
257 warm pool El Niño, *J. Climate*, 22, 1499-1515.

258 Lee, T., and M. J. McPhaden (2010), Increasing intensity of El Niño in the central-equatorial
259 Pacific, *Geophys. Res. Lett.*, 37, L14603, doi:10.1029/2010GL044007.

260 Mo, K. C. (2010), Interdecadal Modulation of the Impact of ENSO on Precipitation and
261 Temperature over the United States, *J. Climate*, 23, 3639–3656, doi: 10.1175/2010JCLI3553.1

262 Moore, A. M., R. Kleeman (1999), The Nonnormal Nature of El Niño and Intraseasonal
263 Variability, *J. Climate*, 12, 2965–2982.

264 Neelin, J.D. et al. (1998), ENSO theory, *J Geophys. Res.*, 103, 14261–14290.

265 Newman, M. (2007), Interannual to decadal predictability of tropical and North Pacific sea
266 surface temperatures, *J. Climate*, 20, 2333-2356.

267 Newman, M., M. A. Alexander, and J. D. Scott (2011), An empirical model of tropical ocean
268 dynamics, *Clim. Dyn.*, in press, doi: 10.1007/s00382-011-1034-0.

269 Newman M., P. D. Sardeshmukh, and C. Penland (2009), How important is air-sea coupling in
270 ENSO and MJO evolution? *J. Climate*, 22, 2958-2977.

271 Penland C., and P. D. Sardeshmukh (1995), The optimal growth of tropical sea surface
272 temperature anomalies, *J. Climate*, 8, 1999–2024.

273 Rayner N. A. et al. (2003), Global analyses of sea surface temperature, sea ice, and night marine
274 air temperature since the late nineteenth century, *J. Geophys. Res.*, *108*, 4407, DOI:
275 10.1029/2002JD002670.

276 Rudnick, D. L., and R. E. Davis (2003), Red noise and regime shifts, *Deep Sea Res. I*, *50*, 691-
277 699.

278 Smith, T. M., and R. W. Reynolds (2004), Improved Extended Reconstruction of SST (1854-
279 1997), *J. Climate*, *17*, 2466-2477.

280 Smith, T. M., R. W. Reynolds, T. C. Peterson, and J. Lawrimore (2008), Improvements to
281 NOAA's Historical Merged Land-Ocean Surface Temperature Analysis (1880-2006), *J. Climate*,
282 *21*, 2283-2296.

283 Solomon, A., and M. Newman (2011), Decadal predictability of tropical Indo-Pacific Ocean
284 temperature trends due to anthropogenic forcing in a coupled climate model, *Geophys. Res. Lett.*,
285 *38*, L02703, doi:10.1029/2010GL045978.

286 Trenberth, K. E., and D. P. Stepaniak (2001), Indices of El Niño evolution, *J. Climate*, *14*, 1697-
287 1701.

288 Wunsch, C. (1999), The interpretation of short climate records, with comments on the North
289 Atlantic and Southern Oscillations, *Bull. Amer. Meteor. Soc.*, *80*, 245-255.

290 Yeh, S-W. et al. (2009), El Niño in a changing climate, *Nature*, *461*, 511-514.

291 Yeh, S.-W, et al. (2010), Natural variability of the central Pacific El Niño event on multi-
292 centennial timescales, *Geophys. Res. Lett.*, *38*, L02704, doi:10.1029/2010GL045886.

293 Yu, J.-Y., and S. T. Kim (2010), Identification of central-Pacific and eastern-Pacific types of
294 ENSO in CMIP3 models, *Geophys. Res. Lett.*, *37*, L15705, doi:10.1029/2010GL044082.

295 Yu, J.-Y., and S. T. Kim (2011), Relationships between extratropical sea level pressure
296 variations and the central Pacific and eastern Pacific types of ENSO, *J. Climate*, *24*, 708-720.

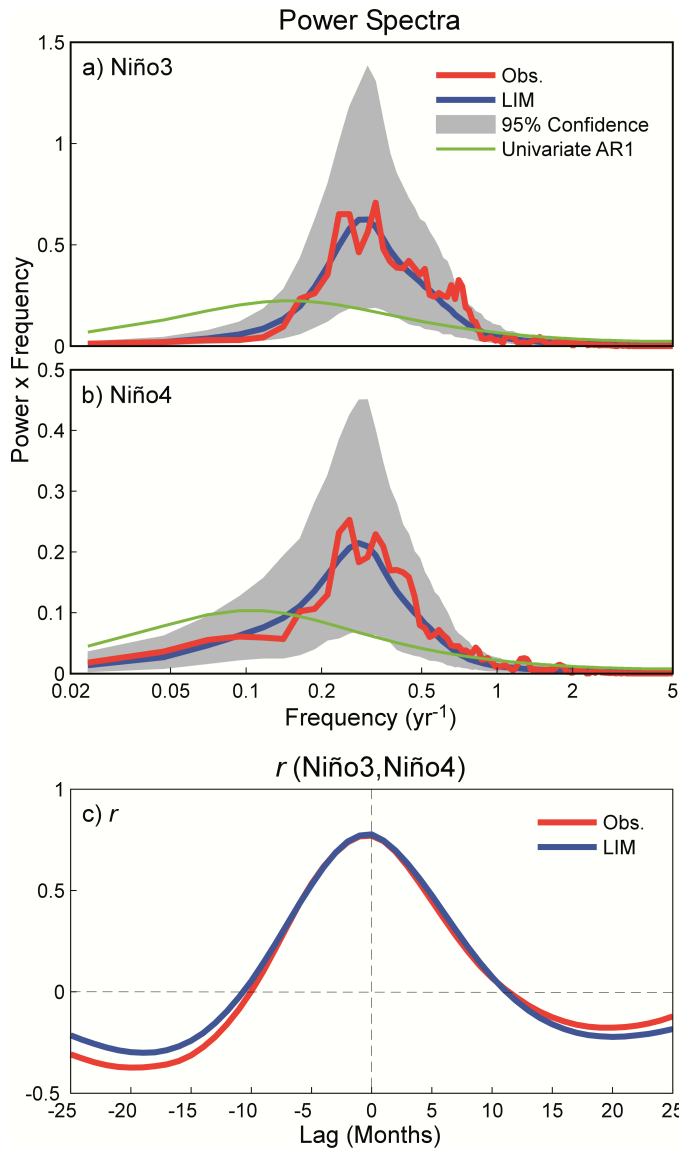
297

Averaging interval (yrs)	$r(\text{Niño3}, \text{Niño4})$	Change in $r(\text{Niño3}, \text{Niño4})$, consecutive intervals	CP/EP ratio	Change in CP/EP ratio, consecutive intervals	% of intervals without CP events
10	0.42 – 0.96	0.44	$0 - \infty$	∞	50
30	0.63 – 0.91	0.20	$0 - 1.2$	0.96	14
30 (10-yr overlap)	0.63 – 0.91	0.13	$0 - 1.2$	0.55	14
50	0.67 – 0.88	0.15	$0 - 0.88$	0.64	3.4
100	0.71 – 0.86	0.11	$0.1 - 0.62$	0.44	0.3

298

299 **Table 1. First four columns: 95% confidence intervals determined from computing r and CP/EP, using different**
 300 **interval sizes, from a 24000 yr forward integration of (2). Last column: the total fraction of intervals that**
 301 **had no CP events.**

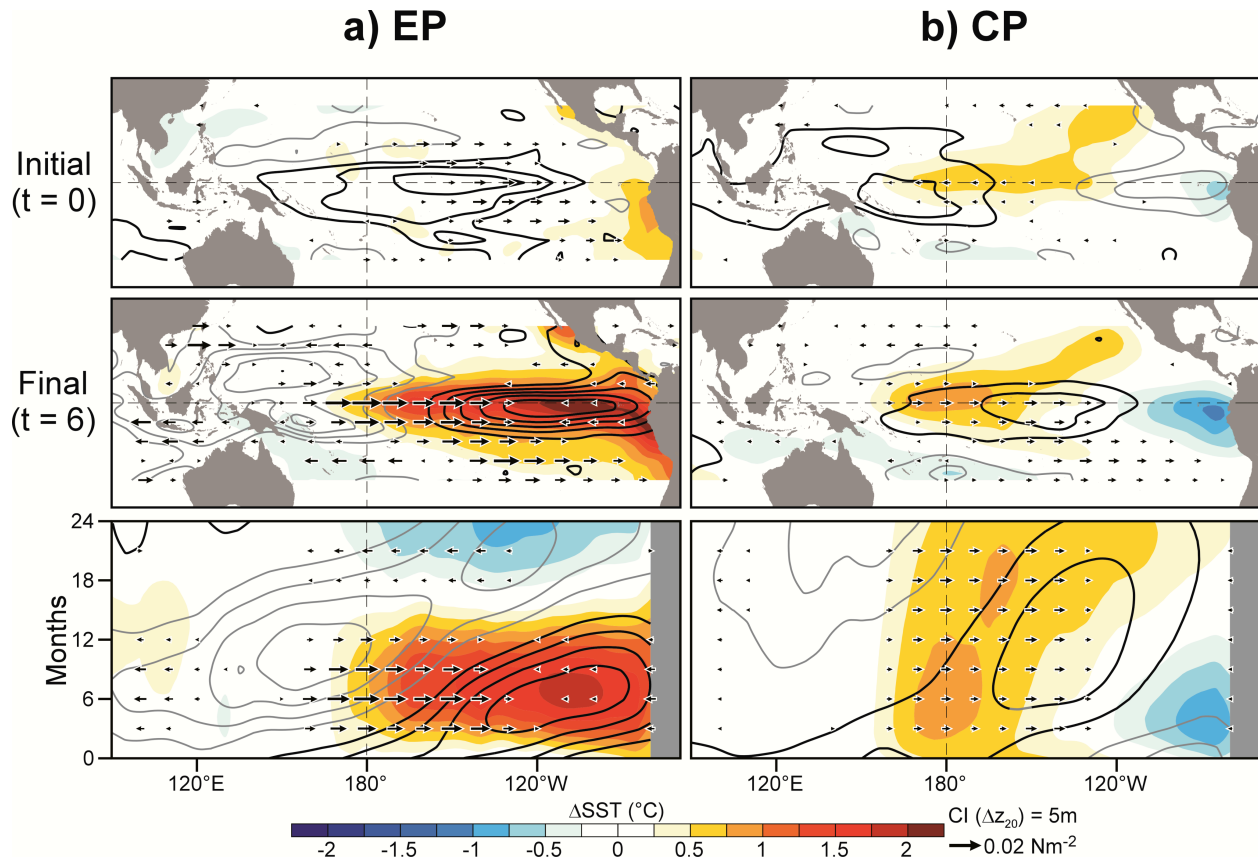
302



304

305 **Figure 1.** Power spectra for the (a) Niño 3 and (b) Niño4 SST indices for the years 1959-2000 (red lines),
 306 compared to those predicted by multivariate red noise (i.e., the LIM; blue lines) and by a univariate red
 307 noise fit (green lines). Gray shading represents the 95% confidence interval determined from a 500-
 308 member ensemble of 42 yr-long LIM forward integrations (see NAS for further details). In these
 309 log(frequency) versus power times angular frequency (ω) plots, the area under any portion of the curve
 310 is equal to the variance within that frequency band. Note that displaying power spectral density slightly
 311 shifts the power spectral density peak centered at a period of 4.5 yrs to a variance peak centered at a
 312 period of 3.5 yrs. (c) Correlation between Niño 3 and Niño 4 indices, for lags ranging up to 25 months.
 313 Positive lags indicate Niño 3 leads Niño 4; negative lags indicate Niño 4 leads Niño 3.

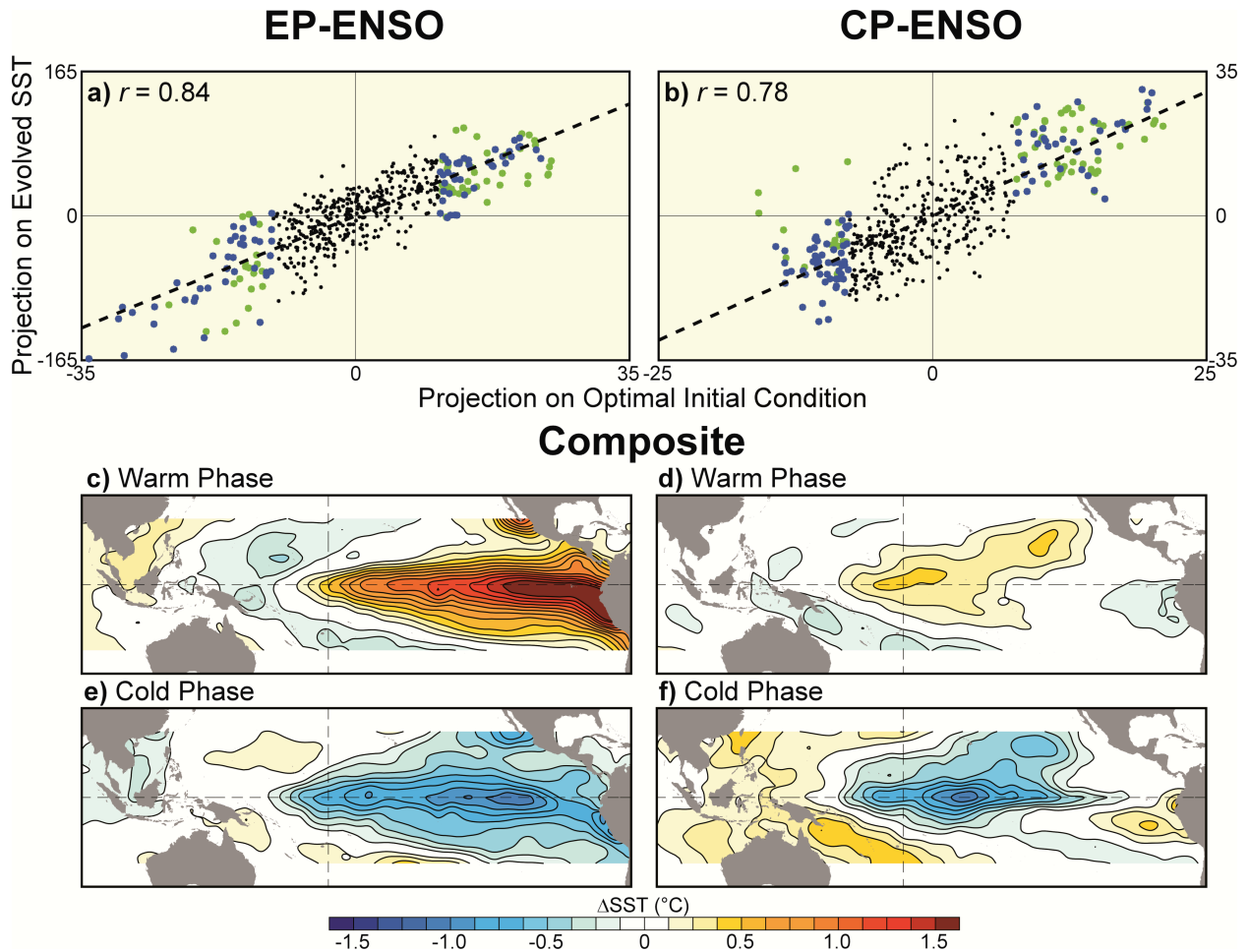
314



315

316 **Figure 2: Leading patterns for SST anomaly amplification over a six-month interval (i.e., optimal structures),**
 317 **determined from a singular vector decomposition of the system propagator $exp(6L)$ under the L2 norm**
 318 **(i.e., domain-mean square amplitude) of anomalous SST. a) Evolution of the first pattern (which leads to**
 319 **an EP-type ENSO), shown as maps at (top) $t = 0$ and (middle) $t = 6$ months, and (bottom) as a time-**
 320 **longitude cross-section of the evolution along the equator. b) Same as (a) except the evolution of the**
 321 **second pattern (which leads to a CP-type ENSO). Anomalous SST is indicated by shading (contour**
 322 **interval 0.25 K), thermocline depth by contours (contour interval 5 m, where black is positive), and**
 323 **zonal wind stress by black vectors (scaled by the reference vector 0.02 Nm^{-2} , with values below 0.002**
 324 **Nm^{-2} removed for clarity). Note that the opposite-signed patterns lead to cold events.**

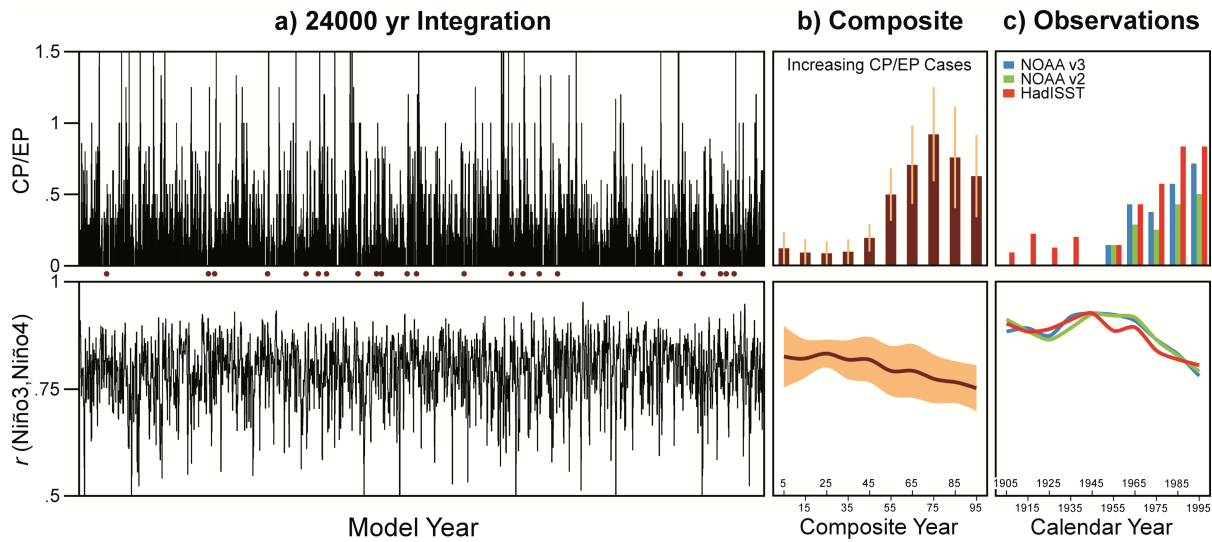
325



326

327 **Figure 3.** Top panels: Projection of observations upon the optimal initial condition for SST anomaly amplification
 328 over a six-month interval, versus the projection on the optimal evolved SST state 6 months later, for (a)
 329 the EP pattern and (b) the CP pattern. Note that the tropical SST growth factor for the EP pattern is
 330 almost 4 times greater than for the CP pattern. Blue dots indicate initial anomalies with large projection
 331 (magnitude greater than 1 standard deviation) on *either* the EP-ENSO or CP-ENSO optimal structure
 332 amplitudes, but not both; green dots indicate initial anomalies with large projection (over 1 standard
 333 deviation) on *both* optimal structures. Bottom panels: HadISST (Rayner *et al.* [2003]) SST composite
 334 anomalies constructed six months following the dates represented by the blue dots. Composites are
 335 constructed separately for (c and d) positive (warm phase) and (e and f) negative (cold phase)
 336 projection values. Anomalies with initially high projection on both optimal patterns (i.e., green dots) are
 337 excluded from the composites.

338



340

341 **Figure 4. Measures of ENSO variations from multivariate red noise compared to observations. (top) CP/EP El Niño**
 342 **(i.e., warm event only) occurrence ratio and (bottom) r (Niño3, Niño4), for (a) the 24000 yr integration,**
 343 **(b) a composite over all the “increasing CP/EP cases” from the integration, with \pm one standard deviation**
 344 **indicated by orange bars/shading, and (c) the SST datasets HadISST (red; *Rayner et al. [2003]*), NOAA v2**
 345 **(green; *Smith and Reynolds [2004]*), and NOAA v3 (blue; *Smith et al. [2008]*) for the years 1891-2010. In**
 346 **all cases the quantities are computed over 30-yr long intervals centered 10 years apart. Years on the**
 347 **abscissa represent the center of the 30-yr interval. The “increasing CP/EP cases,” indicated by dots**
 348 **between top and bottom panels in (a), are two adjacent 60-year segments for which the CP/EP ratio rises**
 349 **from below normal to above normal, and simultaneously r (Niño3, Niño4) decreases, from the first 60-yr**
 350 **segment to the second.**

351